

Steady-state and time-resolved photoluminescence from relaxed and strained GaN nanowires grown by catalyst-free molecular-beam epitaxy

John B. Schlager,^{a)} Kris A. Bertness, Paul T. Blanchard, Lawrence H. Robins, Alexana Roshko, and Norman A. Sanford

National Institute of Standards and Technology, Boulder, Colorado 80305, USA

(Received 16 November 2007; accepted 15 April 2008; published online 24 June 2008)

We report steady-state and time-resolved photoluminescence (TRPL) measurements on individual GaN nanowires (6–20 μm in length, 30–940 nm in diameter) grown by a nitrogen-plasma-assisted, catalyst-free molecular-beam epitaxy on Si(111) and dispersed onto fused quartz substrates. Induced tensile strain for nanowires bonded to fused silica and compressive strain for nanowires coated with atomic-layer-deposition alumina led to redshifts and blueshifts of the dominant steady-state PL emission peak, respectively. Unperturbed nanowires exhibited spectra associated with high-quality, strain-free material. The TRPL lifetimes, which were similar for both relaxed and strained nanowires of similar size, ranged from 200 ps to over 2 ns, compared well with those of low-defect bulk GaN, and depended linearly on nanowire diameter. The diameter-dependent lifetimes yielded a room-temperature surface recombination velocity S of 9×10^3 cm/s for our silicon-doped GaN nanowires. [DOI: 10.1063/1.2940732]

I. INTRODUCTION

Gallium nitride (GaN)-based semiconductors have successfully been incorporated into commercial light emitting diodes and commercial laser diodes that operate from ultraviolet (UV) to green wavelengths.¹ $\text{Al}_x\text{Ga}_{1-x}\text{N}$ and $\text{In}_x\text{Ga}_{1-x}\text{N}$ alloys offer the potential to extend the wavelength range of GaN-based photonic devices to the deep UV and into the near infrared.^{2,3} These attributes make GaN a very attractive material for optical sources and optical sensors, but material quality remains an important issue. Conventional growth methods on lattice mismatched substrates produce material with a relatively high density of defects that decrease device yield and increase device cost. Growing GaN in the form of nanowires with catalyst-free molecular-beam epitaxy (MBE), however, can produce strain-free crystalline material with very low-defect density and in a morphology useful for optoelectronic, electronic, and even nanomechanical applications.^{4–6} Optical characterization of these nanowires yields information about the intrinsic material properties, the sensitivity of the material to environmental changes, and the nanowire structure itself. We have performed steady-state and time-resolved photoluminescence (TRPL) measurements on individual GaN nanowires grown by the catalyst-free MBE after wire dispersal and other wire treatments. These measurements give steady-state PL spectra that indicate high-quality, strain-free material. The spectral features respond predictably to changes in temperature and strain. TRPL results show nanosecond decay times comparable to those of high-quality bulk GaN despite the nonradiative surface recombination effects present in these thin nanowires.

We expect this optical characterization as well as ongoing optoelectronic characterization to aid in nanowire optoelectronic device development.

II. EXPERIMENTAL

Nanowires were grown on Si (111) substrates by nitrogen-plasma-assisted MBE with elemental Ga and Al sources.⁴ An AlN buffer layer of 50–100 nm preceded GaN growth and ultimate spontaneous nanowire formation along the polar c -axis direction. The nanowires were removed from the growth substrate and subsequently dispersed onto fused quartz substrates for luminescence measurements. A photolithographically defined, indexed metal grid aided in the identification and location of individual wires. The dispersed nanowires were up to 20 μm in length and 30–500 nm in diameter as determined by field-emission scanning electron microscope (FESEM) image measurements.

For both the PL and TRPL measurements, the dispersed nanowire samples were placed in a continuous-flow cryostat that enabled close optical access and maintenance of stable temperatures from ~ 5 to 296 K. An optical microscope was used to indirectly image individual nanowires in phase contrast to determine location and wire orientation. For steady-state PL, the nanowire samples were excited with a cw HeCd laser operating at 325 nm (3.185 eV) that was focused with a singlet lens to a spot diameter of 4 μm . Steady-state PL spectra were collected with a scanning 0.5 m monochromator that dispersed the luminescence onto an UV-sensitive photomultiplier tube (PMT). The range of excitation intensities was from 50 W/cm² to 10 kW/cm². Unlike PL on bulk material, the cross-sectional area of excited material is set by the dimensions of the individual nanowire and not by the beam spot size. The PL intensity from an individual wire is one to three orders of magnitude less than that of the bulk

^{a)}Author to whom correspondence should be addressed. Electronic mail: schlager@boulder.nist.gov.

material with an equivalent excitation spot. For this reason, typical steady-state excitation intensities exceeded 500 W/cm^2 to maintain an adequate signal-to-noise ratio for sufficiently rapid scan times (less than 10 min). The excitation source in the TRPL experiments was a frequency-tripled, mode-locked Ti:sapphire laser operating at 266 nm (4.66 eV) at a repetition rate of 2 MHz. Again, spectra were collected with a scanning monochromator, but the TRPL work used a fast, UV-sensitive, PMT-amplifier combination that provided electrical pulse delay information for time-correlated single-photon counting (TCSPC) electronics. Together with a computer, the TCSPC electronics enabled display of the temporal response of nanowire PL. The temporal resolution (with reconvolution) was $\sim 100 \text{ ps}$. The maximum pulse fluence was $260 \mu\text{J/cm}^2$ with corresponding intensities exceeding 100 MW/cm^2 . Photoluminescent spectra obtained from steady-state HeCd excitation and those obtained through time-integrated TRPL measurements were in good agreement. The photon energies of peak PL emission were within 1 meV for the two systems, and the measured linewidths were within a few meV.

Steady-state PL was performed on short (less than $10 \mu\text{m}$) and long ($>10 \mu\text{m}$) nanowires that were simply dispersed onto quartz substrates. Nanowires that were conformally coated with alumina (Al_2O_3) by atomic-layer deposition (ALD) prior to dispersal were also examined (ALD coatings were studied as potential surface passivation layers).⁷ These nanowire treatments introduced varying amounts of strain that became evident via shifts in the PL spectra at various temperatures. TRPL measurements were performed on both dispersed and as-grown nanowires.

III. RESULTS AND DISCUSSION

At base temperature ($\sim 5 \text{ K}$), the shorter ($<10 \mu\text{m}$) randomly dispersed and unintentionally doped GaN nanowires (from growth run B738) produced steady-state PL spectra with the dominant donor-bound exciton D^0X_A peak at 3.472 eV (corresponding to strain-free GaN)⁶ and a linewidth of 5 meV full width at half maximum. The spectral peaks associated with the free A and B excitons also occurred at their expected strain-free positions of 3.478 and 3.483 eV, respectively, as shown in Fig. 1. As with other MBE-grown nanowires and unlike GaN nanowires grown by metal-organic chemical vapor deposition, no yellow luminescence associated with structural defects or impurities was observed in our PL spectra of individual wires.^{8,9} The excitation intensity at 325 nm for these data was 550 W/cm^2 .

The longer and thicker (greater than $10 \mu\text{m}$ in length and greater than 300 nm in diameter), randomly dispersed nanowires exhibited increasingly redshifted PL peaks and spectral broadening with cooling. At base temperature, the dominant PL peak position for a silicon-doped GaN (GaN:Si , $N_d = 6 \pm 2 \times 10^{17} \text{ cm}^{-3}$) nanowire $12.7 \mu\text{m}$ long and 425 nm in diameter (from growth run B982) was $3.462 \pm 0.002 \text{ eV}$ with excitation intensities below 500 W/cm^2 (Fig. 2). However, using x-ray diffraction on the as-grown material, we found the measured room-temperature *a*-axis and *c*-axis lattice constants ($a = 0.3189 \pm 0.0001 \text{ nm}$ and c

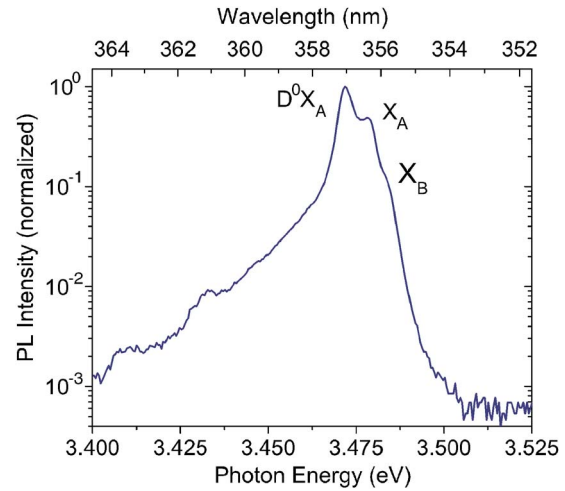


FIG. 1. (Color online) Low-temperature ($\sim 5 \text{ K}$) steady-state PL spectrum of an unintentionally doped $6 \mu\text{m}$ long B738 GaN nanowire of 60 nm diameter. The excitation intensity was 550 W/cm^2 at 325 nm . X_A —A free exciton, X_B —B free exciton, and D^0X_A —donor-bound A exciton.

$= 0.5185 \pm 0.00004 \text{ nm}$) of these B982 nanowires to be consistent with those of strain-free bulk GaN published elsewhere.¹⁰ These results suggest that the PL shift was due to a differential thermal contraction of the dispersed B982 nanowire relative to the quartz substrate—the net result leading to a tensile strain of the nanowire upon cooling. If we use the coefficients of the linear thermal expansion, $\alpha(T)$, for GaN and fused silica,^{11,12} we can calculate the fractional length changes expected for these materials with a change in temperature,

$$\frac{\Delta L_{T_2-T_1}}{L_{T_1}} = \int_{T_1}^{T_2} \alpha(T) dT, \quad (1)$$

where T_1 and T_2 are the starting and ending temperatures, respectively. Assuming a perfect van der Waals bond between the fused silica substrate and the nanowire, we can then calculate the strain for both the *c*-axis (ϵ_{zz} , \parallel nanowire)

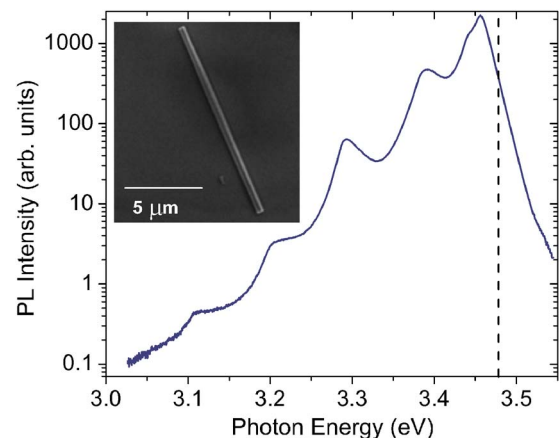


FIG. 2. (Color online) Low-temperature ($\sim 5 \text{ K}$) steady-state PL spectrum of a B982 Si:GaN nanowire $12.7 \mu\text{m}$ long and 425 nm in diameter dispersed on a fused silica substrate. The vertical dashed line indicates the strain-free position of donor-bound A exciton, D^0X_A , peak. Lower energy satellite peaks represent LO-phonon mediated transitions. HeCd (325 nm) excitation intensity is $\sim 3 \text{ kW/cm}^2$. Inset: FESEM image of a dispersed B982 Si:GaN nanowire, $12.7 \mu\text{m}$ length and 425 nm diameter.

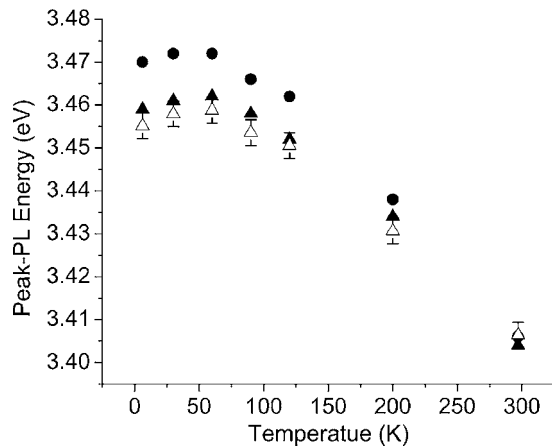


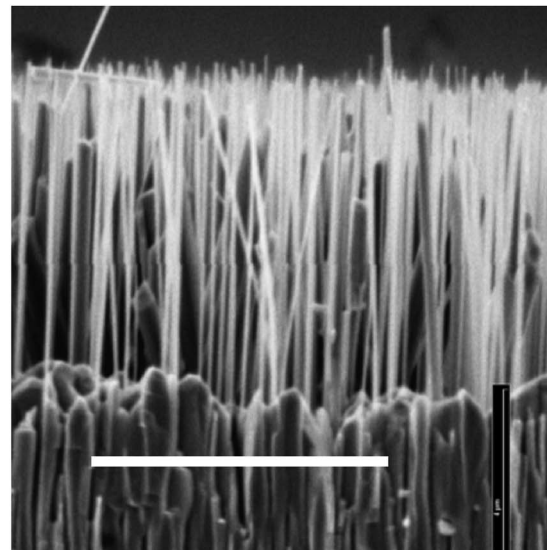
FIG. 3. Measured peak PL energies for the dispersed B738 nanowire (closed circles) and the dispersed B982 nanowire (closed triangles) as functions of temperature. The expected peak PL energies for the B982 nanowires are also shown (open triangles with error bars). These energies were determined by calculating the temperature-dependent bandgap shifts using Eqs. (1) and (2) and adding these shifts to the B738 nanowire data, which are considered to be strain-free.

and a -axis ($\epsilon_{xx} = \epsilon_{yy}$, \perp nanowire) directions. Combining this information with the deformation potentials for GaN from Peng *et al.*,¹³ we can calculate the expected bandgap shift for the A exciton due to the temperature change from 295 to 5 K on our dispersed nanowires,

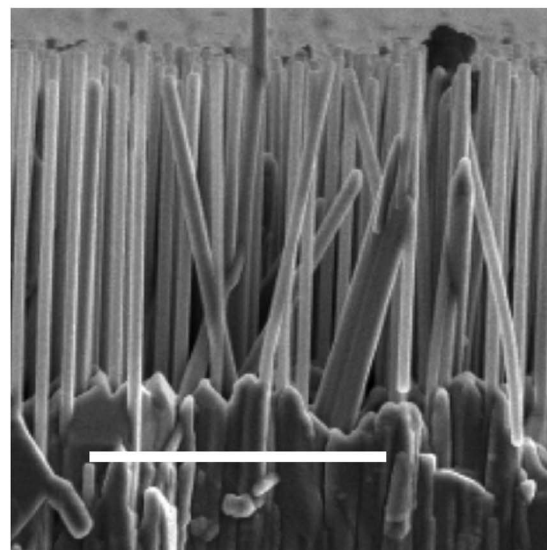
$$\begin{aligned} \Delta E_A &= (a_{cz} - D_1)\epsilon_{zz} + (a_{ct} - D_2)(\epsilon_{xx} + \epsilon_{yy}) \\ &\quad - D_3\epsilon_{zz} - D_4(\epsilon_{xx} + \epsilon_{yy}) \\ &= -13 \pm 3 \text{ meV}, \end{aligned} \quad (2)$$

where a_{cz} and a_{ct} are the conduction band deformation potentials, and D_1 , D_2 , D_3 , and D_4 are the valence band deformation potentials.¹³ This calculated bandgap shift agrees (within uncertainty) with the observed shift in the D^0X_A peak at ~ 5 K (-10 ± 2 meV) shown in Fig. 2. Doing the same calculation at different temperatures, we find that the expected bandgap shifts match the observed shifts in peak PL energy between that of a strain-free B738 nanowire and that of a longer B982 nanowire bonded to fused silica. The measured peak PL energies for the two nanowires are plotted in Fig. 3 with those calculated for the longer B982 nanowire bonded to fused silica.

Conformal coating of the nanowire with ALD alumina introduced compressive strain and a blueshift in the PL spectral peak. Figure 4 shows FESEM images of (a) uncoated and (b) coated B738 nanowires still attached to their growth substrates. The thickness of the alumina coating was 70 nm. Figure 5(a) shows the normalized room-temperature PL spectra with a $+35 \pm 3$ meV blueshift in the spectral peak. Photoluminescent intensities for both coated and uncoated wires were equivalent (within the normal wire-to-wire variation of PL output) indicating negligible absorption due to the thin alumina coating. X-ray diffraction recorded before and after ALD alumina coating showed a decrease in a and c lattice constants with $\Delta a = -37 \pm 32 \times 10^{-5}$ nm and $\Delta c = -16 \pm 3 \times 10^{-5}$ nm. The associated a - and c -axis strains were $\epsilon_{xx} = -12 \pm 7 \times 10^{-4}$ and $\epsilon_{zz} = -3 \pm 1 \times 10^{-4}$, respec-



(a)



(b)

FIG. 4. (a) FESEM image of as-grown B738 GaN nanowires. (b) FESEM image of ALD coated B738 nanowires with 70 nm conformal alumina coating. Scale bars indicate 5 μm length.

tively. The lattice constants were calculated for both ALD coated and uncoated cases using the 2θ peak positions of the (0 0 0 2), (0 0 0 4), (0 0 0 6), (1 0-1 4), (1 0-1 5), and (2 0-2 4) reflexes [see, e.g., Fig. 5(b)]. With the deformation potentials and relations of Peng *et al.*,¹³ we calculated the associated energy bandgap shifts to be $\Delta E_A = 21 \pm 11$ meV, $\Delta E_B = 26 \pm 12$ meV, and $\Delta E_C = 43 \pm 12$ meV. These values are consistent with the observed room-temperature shift for the spectral peak seen in Fig. 5, which comprises a convolution of the three free exciton peaks (A , B , and C). Surprisingly, the a - and c -axis strains can also be estimated by using the room-temperature coefficients of linear thermal expansion α for GaN and bulk alumina ($\alpha_{\text{alumina}} = 7 \pm 1 \times 10^{-6}$ K⁻¹, $\alpha_{c\text{-GaN}} = 3.8 \pm 0.4 \times 10^{-6}$ K⁻¹, $\alpha_{a\text{-GaN}} = 4.0 \pm 0.4 \times 10^{-6}$ K⁻¹) (Refs. 10 and 14) to calculate the expected fractional length change for a temperature change from the ALD deposition temperature (175 °C) to room temperature (22 °C). Doing

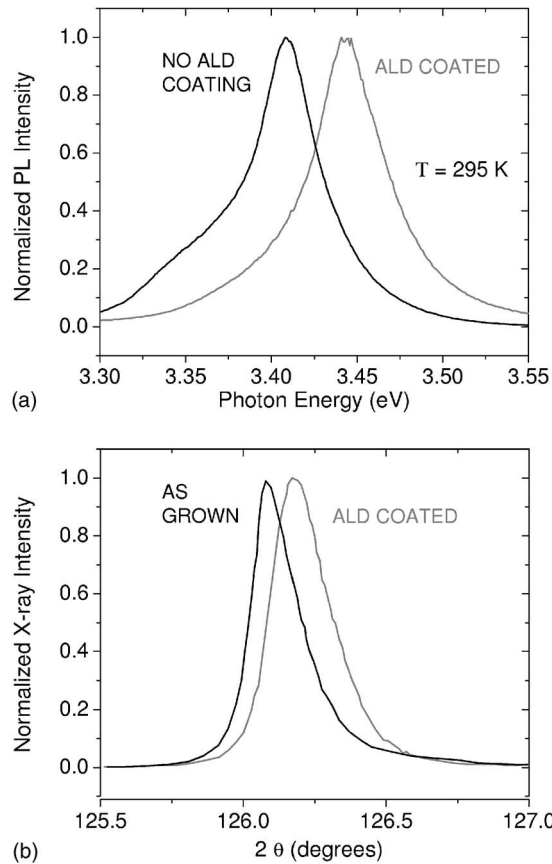


FIG. 5. (a) PL spectrum of the B738 GaN nanowire at 295 K with and without ALD alumina coating; (b) example (0 0 0 6) ω -2 θ x-ray diffraction for as-grown (no ALD) and ALD alumina-coated nanowires.

so yields strain values of $\varepsilon_{xx}=\varepsilon_{yy}=-11\pm 2\times 10^{-4}$ and $\varepsilon_{zz}=-5\pm 2\times 10^{-4}$, which agree, within uncertainty, with the values determined solely from x-ray diffraction measurements above. This result may be pure coincidence since there is no reason that ALD alumina should necessarily behave like bulk alumina. The associated bandgap shifts here are $\Delta E_A=22\pm 6$ meV, $\Delta E_B=27\pm 5$ meV, and $\Delta E_C=44\pm 5$ meV, which, again, are consistent with the observed PL peak shift.

TRPL measurements on individually dispersed and as-grown GaN nanowires gave PL decay times from ~ 200 ps to ~ 2.7 ns that depended on the temperature and nanowire diameter. Figure 6 shows the temporal decay of PL at three temperatures for the same dispersed B982 GaN:Si nanowire pictured in the inset of Fig. 2. Although the curves exhibited evidence of more than one decay process, each curve was fit to a single-exponential decay for best fitting results. Improving the temporal resolution of the TRPL setup to below 100 ps should increase the contrast between decay processes, and a more complex fitting routine may be required. Nevertheless, PL decay processes with decay times exceeding 2 ns were evident in these nanowires. Such decay times compare favorably with PL decay times and carrier lifetimes observed in high-quality bulk GaN with threading dislocation densities at or below 10^6 cm $^{-2}$.^{15,16} Measurements also show that PL decay times depend on the nanowire diameter as detailed below.

To compare the time response of relaxed and strained

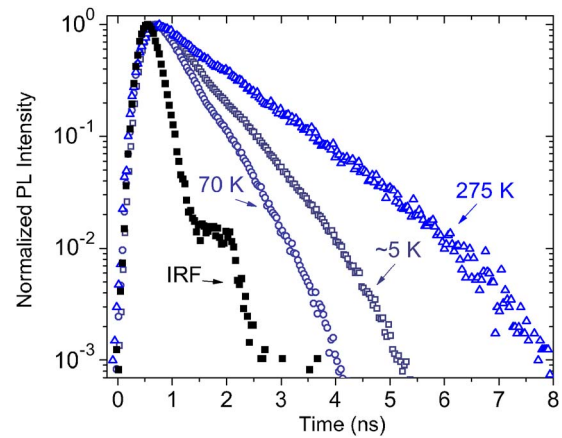


FIG. 6. (Color online) PL temporal decays for the B982 GaN nanowire pictured in the inset of Fig. 2 at three temperatures. Decay times, derived from single-exponential fits, are 660 ps, 470 ps, and 1.17 ns at ~ 5 , 70, and 275 K, respectively. Excitation was at 266 nm (4.66 eV) with $66\ \mu\text{J}/\text{cm}^2$ pulse fluence. The detection wavelengths (energies) were 359 nm (3.45 eV) at $T\sim 5$ K and 363 nm (3.41 eV) at $T\sim 275$ K. The instrument response function is also shown (closed squares).

nanowires of similar size, we performed TRPL measurements on as-grown B982 nanowires still attached to their silicon growth substrates. This was accomplished by placing a section of a silicon wafer into the cryostat with the wafer mounted at an angle so that the UV excitation light could access the approximately 12 μm long nanowires protruding from the wafer edge. As expected, the as-grown nanowires were strain-free with a peak PL occurring at 3.472 eV, corresponding to the donor-bound exciton D^0X_A peak. Photoluminescent decay times as a function of temperature for the as-grown B982 nanowires and the dispersed B982 nanowire (pictured in the inset of Fig. 2) are shown in Fig. 7. TRPL data were collected at the photon energy of peak PL emission for each temperature. This energy ranged from 3.472 eV at $T\sim 5$ K to 3.39 eV at room temperature. Single exponential fits were used to determine decay times. No significant difference is seen between the temperature-dependent PL decay

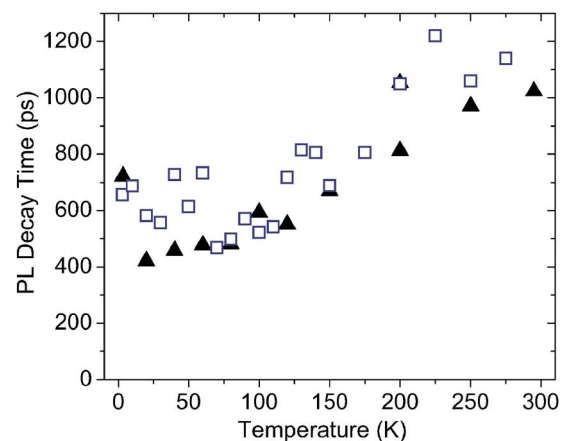


FIG. 7. (Color online) PL decay time vs temperature for the dispersed B982 nanowire (open squares) and as-grown B982 nanowires (closed triangles). The excitation pulse fluence for the dispersed nanowire (as-grown nanowires) measurement was $106\ \mu\text{J}/\text{cm}^2$ (210 ± 50 mJ/cm 2). Decay times were collected at the photon energy of peak PL emission for each temperature.

times for the relaxed and strained B982 nanowires. Although the scatter in Fig. 7 data is significant, the slight decrease in PL decay time from base temperature to ~ 70 K (also evident in Fig. 6) was reproducible. We believe that this decrease is due to a thermally activated increase in the nonradiative decay rate, which is related to the dissociation of the exciton from the neutral donor.¹⁷ Above ~ 70 K, the PL decay time increases in temperature but at a rate (particularly above 125 K) that is less than expected for a purely radiative carrier recombination.¹⁸

The highly photoexcited B982 GaN nanowires within the TRPL setup (excitation fluences ~ 100 – $260 \mu\text{J}/\text{cm}^2$) gave time-integrated PL spectra with evidence of inelastic exciton-exciton collision at cold temperatures and evidence of electron-hole plasma (EHP) at room temperature. The presence of two separate recombination processes (exciton and EHP) with a temperature-dependent transition from one to the other was earlier observed by Herzog *et al.*¹⁹ in their spectroscopic study of stimulated emission in GaN. Exciton-exciton collision in the B982 nanowires gave rise to a broad luminescence peak that appeared as a shoulder on the low-energy side of the PL peak at 3.460 eV, the so-called *P* band, from $T \sim 5$ K up to 40 K.²⁰ The room-temperature, time-integrated PL exhibited a quadratic dependence of spectrally integrated emission intensity on excitation fluence that is typical of radiative recombination in a dense EHP, expected to exist here, particularly for times within ~ 1 ns of the excitation pulse.²¹ A slight room-temperature redshift in peak PL emission was also observed with increased excitation intensity, but this spectral shift was not accompanied by a narrowing in the PL emission linewidth. This effect, which was more pronounced for light emanating from the wire ends, was attributed to band reabsorption effects and not stimulated emission. In separate experiments, we have seen spectral narrowing with increased excitation fluence and optically pumped lasing action in these nanowires, but these occur at fluences around $\sim 1 \text{ J}/\text{cm}^2$, much greater than those used here.

The average PL decay time of around 550 ps for the D^0X_A peak (3.472 eV at $T \sim 5$ K) reported here was close to the 530 ps decay time observed by Bunea *et al.*²² for cold D^0X_A emission in high-quality, 63 μm thick, GaN film grown by hydride vapor phase epitaxy (HVPE). The PL decay time at room temperature of ~ 1.1 ns was in good agreement with the PL decay time observed by Jursenas *et al.*²¹ in high-quality, 100 μm thick, HVPE grown GaN under strong two-photon (2P), i.e., 532 nm/2.33 eV pump, excitation conditions. This was despite the fact that all nanowire diameters were under 1 μm . 2P excitation of bulk GaN takes advantage of the much greater penetration depth of these sub-bandgap pump photons and avoids the carrier diffusion effects associated with single-photon (1P) surface excitation, which can introduce fast transients into the PL decay data obtained with 1P excitation.^{21,23} The PL decay data with 1P excitation for our nanowires, however, do not suffer from the impact of carrier diffusion. This is because the nanowire diameters are small compared to the carrier diffusion lengths traveled over the nanosecond decay times. Both 1P excitation

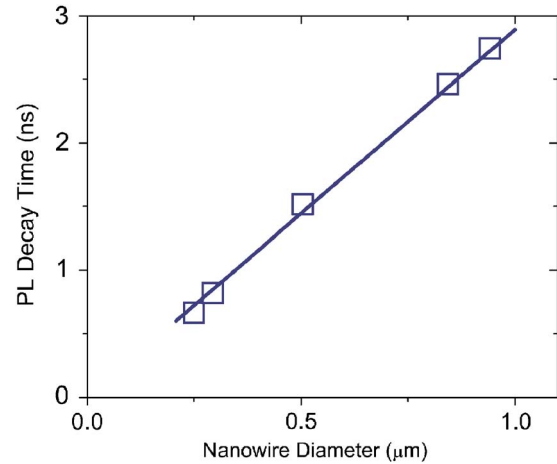


FIG. 8. (Color online) Room-temperature PL decay time vs the nanowire diameter for the B982 GaN:Si nanowires. The open squares represent data and the solid line represents the best linear fit. From the slope of this line, we calculate the surface recombination velocity $S \sim 9 \times 10^3 \text{ cm/s}$ (see text).

and sub-bandgap multiphoton excitation (pump at 800 nm or 1.55 eV) of our nanowires yield similar room-temperature PL decay times.

As mentioned above, the PL decay times depended on the nanowire diameter. We measured the room-temperature PL decay for five separate B982 GaN:Si nanowires with diameters varying from 250 to 940 nm. The lengths of these wires were $13 \pm 2 \mu\text{m}$. The nanowires were dispersed on fused quartz and placed in the evacuated cryostat to avoid any variability associated with the changing atmosphere. As seen in Fig. 8, we found that the room-temperature PL decay times depended linearly on the nanowire diameter, indicating that the observed lifetimes are determined by the nonradiative surface recombination. For nanowires with a cylindrical cross section, the nonradiative surface recombination lifetime is $\tau_s \sim d/4S$, where d is the wire diameter and S is the surface recombination velocity. This formula matches the surface recombination time expected for a filament with a square cross section,²⁴ but it differs from the formula expected for a planar confinement structure ($\tau_s \sim d/2S$), where the planar active layer (of thickness d) is bound by only two surfaces/interfaces.¹⁸ We assume that $\tau_s \sim d/4S$ applies to our GaN nanowires with hexagonal cross sections. Fitting a line to the data of Fig. 8, we find from the slope ($1/4S$) that the room-temperature surface recombination velocity is $S \sim 9 \times 10^3 \text{ cm/s}$. This value is over five times smaller than that reported for undoped GaN epilayers and is over 100 times smaller than that reported for GaAs ($S \sim 10^6 \text{ cm/s}$).^{25,26} The low surface recombination velocity and long carrier decay times make this nanowire material a good candidate for nanoscale optoelectronic device applications where the surface to volume ratios for the active materials will necessarily be large.

IV. CONCLUSIONS

In conclusion, steady-state PL measurements on GaN nanowires grown by nitrogen-plasma-assisted, catalyst-free MBE yield well understood PL spectra that respond predictably to changes in strain induced by nanowire dispersal and

bonding to substrates as well as strain due to ALD surface treatments. The TRPL lifetimes that can exceed 2 ns are similar for both relaxed and strained nanowires and compare well with those of low-defect bulk GaN at both low temperature where the D^0X_A emission dominates the PL spectrum and at room-temperature where, under our TRPL excitation conditions, an EHP exists. This is true despite submicron diameters of these nanowires, because the emission dynamics in this MBE-grown GaN material are relatively insensitive to surface states as indicated by the relatively low surface recombination velocity of 9×10^3 cm/s.

These characteristics make these MBE-grown GaN nanowires good candidates for optoelectronic applications at the nanoscale.

ACKNOWLEDGMENTS

We gratefully acknowledge partial support from the DARPA Center for Integrated Micro/Nano-Electromechanical Transducers (*iMINT*) funded by DARPA S&T Fundamentals Program (Award No. HR0011-06-1-0048). We thank Beau B. Burton and Steven M. George of the Department of Chemistry and Biochemistry at the University of Colorado at Boulder for providing and depositing the ALD coatings.

¹S. Nakamura, S. Pearson, and G. Fasol, *The Blue Laser Diode* (Springer, New York, 2000).

²*III-Nitride Semiconductors Optical Properties I, Optoelectronic Properties of Semiconductors and Superlattices*, edited by M. O. Manasreh and H. X. Jiang (Taylor & Francis, New York, 2002).

³B. Monemar, P. P. Paskov, J. P. Bergman, A. A. Toropov, and T. V. Shubina, *Phys. Status Solidi B* **244**, 1759 (2007).

⁴K. A. Bertness, A. Roshko, N. A. Sanford, J. M. Barker, and A. V. Davydov, *J. Cryst. Growth* **287**, 522 (2006).

⁵K. A. Bertness, A. Roshko, L. M. Mansfield, T. E. Harvey, and N. A.

Sanford, *J. Cryst. Growth* **300**, 94 (2007).

⁶J. B. Schlager, N. A. Sanford, K. A. Bertness, J. M. Barker, A. Roshko, and P. T. Blanchard, *Appl. Phys. Lett.* **88**, 213106 (2006).

⁷J. W. Elam, M. D. Groner, and S. M. George, *Rev. Sci. Instrum.* **73**, 2981 (2002).

⁸L. Cerutti, J. Ristic, S. Fernandez-Garrido, and E. Calleja, *Appl. Phys. Lett.* **88**, 213114 (2006).

⁹G. T. Wang, A. A. Talin, D. J. Werder, J. R. Creighton, E. Lai, R. J. Anderson, and I. Arslan, *Nanotechnology* **17**, 5773 (2006).

¹⁰S. Porowski, *J. Cryst. Growth* **189**, 153 (1998).

¹¹C. Roder, S. Einfeldt, S. Figge, and D. Hommel, *Phys. Rev. B* **72**, 085218 (2005).

¹²Standard Reference Materials—Historical Archived Certificates—SRM 739 (<http://ts.nist.gov/MeasurementServices/ReferenceMaterials>).

¹³H. Y. Peng, M. D. McCluskey, Y. M. Gupta, M. Kneissl, and N. M. Johnson, *Phys. Rev. B* **71**, 115207 (2005).

¹⁴Material Property Data (<http://www.matweb.com>).

¹⁵T. Malinauskas, R. Aleksiejunas, K. Jarasiunas, B. Beaumont, P. Gibart, A. Kakanakova-Georgieva, E. Janzen, D. Gagova, B. Monemar, and M. Heuken, *J. Cryst. Growth* **300**, 223 (2007).

¹⁶S. F. Chichibu, A. Uedono, T. Onuma, T. Sota, B. A. Haskell, S. P. DenBaars, J. S. Speck, and S. Nakamura, *Appl. Phys. Lett.* **88**, 021914 (2006).

¹⁷G. Pozina, J. P. Bergman, T. Paskova, and B. Monemar, *Appl. Phys. Lett.* **75**, 4124 (1999).

¹⁸R. K. Ahrenkiel, in *Minority Carriers in III-V Semiconductors: Physics and Applications* (Academic Press, Boston, 1993), Vol. 39, pp. 39–150.

¹⁹W. D. Herzog, G. E. Bunea, M. S. Unlu, B. B. Goldberg, and R. J. Molnar, *Appl. Phys. Lett.* **77**, 4145 (2000).

²⁰L. Eckey, J. C. Holst, A. Hoffmann, I. Broser, T. Detchprohm, and K. Hiramatsu, *MRS Internet J. Nitride Semicond. Res.* **2**, 1 (1997).

²¹S. Jursenas, S. Miasojedovas, A. Zukauskas, B. Lucznik, I. Grzegory, and T. Suski, *Appl. Phys. Lett.* **89**, 172119 (2006).

²²G. E. Bunea, W. D. Herzog, M. S. Unlu, B. B. Goldberg, and R. J. Molnar, *Appl. Phys. Lett.* **75**, 838 (1999).

²³T. Malinauskas, K. Jarasiunas, S. Miasojedovas, S. Jursenas, B. Beaumont, and P. Gibart, *Appl. Phys. Lett.* **88**, 202109 (2006).

²⁴W. Shockley, *Electrons and Holes in Semiconductors* (Van Nostrand, New York, 1950).

²⁵R. Aleksiejunas, M. Sudzius, T. Malinauskas, J. Vaitkus, K. Jarasiunas, and S. Sakai, *Appl. Phys. Lett.* **83**, 1157 (2003).

²⁶J. Lloyd-Hughes, S. K. E. Merchant, L. Fu, H. H. Tan, C. Jagadish, E. Castro-Camus, and M. B. Johnston, *Appl. Phys. Lett.* **89**, 232102 (2006).